

Contents lists available at ScienceDirect

# Journal of Energy Chemistry



journal homepage: www.elsevier.com/locate/jechem

# Research article

# A protein-enabled protective film with functions of self-adapting and anion-anchoring for stabilizing lithium-metal batteries

Chenxu Wang, Xuewei Fu\*, Shengnan Lin, Jin Liu, Wei-Hong Zhong\*

School of Mechanical and Materials Engineering, Washington State University, Pullman, WA 99164, USA

#### ARTICLE INFO

Article history: Received 21 April 2021 Revised 10 May 2021 Accepted 11 May 2021 Available online 21 May 2021

Keywords: Zein Self-adapting Flexibility Lithium metal Lithium dendrite

# ABSTRACT

Practical implementations of rechargeable lithium (Li) metal batteries have long been plagued by multiple problems of Li anode, such as Li dendrite growth, large volume change, low Coulombic efficiency. Here, we report a protein-enabled film that can provide effective protection for Li metal. The protective film with an integrated design of high flexibility, strong adhesion and high Li-ion transference number (0.80) is fabricated by incorporating denatured zein (corn protein) with polyethylene oxide (PEO) acting as an agent for sustaining the denatured protein chains against refolding via the intermolecular interactions between them. Thus, a conformable zein-enabled protective film (zein@PEO) with simultaneous enhancement in flexibility, modulus and adhesion strength is generated to offer both functions of self-adapting and anion-anchoring abilities. The results show that the zein@PEO film is able to accommodate the volume change, reduce the side reactions, and homogenize the ion deposition. Benefiting from these significant properties/functions, the Li/Cu cell with the zein@PEO film delivers prolonged cycle life for over 500 hours with stable performance. Paired with LiMn $_2O_4$  cathode, the capacity, cycle stability and rate performance of the cell are remarkably improved as well, demonstrating the effectiveness in stabilizing Li metal batteries.

© 2021 Science Press and Dalian Institute of Chemical Physics, Chinese Academy of Sciences. Published by ELSEVIER B.V. and Science Press. All rights reserved.

#### 1. Introduction

The ever-growing demands for high-energy-density power systems have stimulated the pursuit of advanced battery technologies. Lithium (Li) metal, featuring an ultrahigh theoretical specific capacity (3860 mAh g<sup>-1</sup>) and the lowest electrochemical potential (-3.045 V vs. the standard hydrogen electrode), has been regarded as a "Holy Grail" anode for next-generation rechargeable battery systems [1,2]. However, implementing Li anode in reality faces several persistent challenges, such as the growth of Li dendrites, infinite volume change of Li, unstable solid electrolyte interphase (SEI) layer, low Coulombic efficiency, etc. [3]. Particularly, the uncontrollable growth of Li dendrites coupled with the fracture of SEI is considered as the most critical issues, which generate not only "dead" Li species with a capacity decay, but also separator piercing causing internal short circuit and thermal runaway [4].

Suppressing the dendrite growth is the principal task to stabilize the Li anode, and one of the promising strategies is to build a protective film on the anode surface [5]. A variety of protective

 $\label{eq:conditional} \textit{E-mail} \quad \textit{addresses:} \quad \text{xuewei.fu@wsu.edu} \quad \text{(X. Fu),} \quad \text{katie\_zhong@wsu.edu} \quad \text{(W.-H. Zhong)}.$ 

films have been reported and showed superior performance, such as fluorinated polymer film [6], Al<sub>2</sub>O<sub>3</sub> layer [7] and Sn/Li alloy layer [8]. However, the infinite volume deformation and relatively high modulus of Li (shear modulus: 3.7 GPa) [9] incur a tough requirement on the mechanical properties of the protective film, that is, simultaneous achievement of mechanical flexibility and robustness. In such a case, increasing the modulus of the protective films is considered as the most common solution [10]. Yet the minimum shear modulus for mechanically suppressing the dendrite growth, 1 GPa [11], is still a significant obstacle especially for organic films. Although some protective films showing extremely high modulus have been reported recently, such as Nafion/LiCl (6.12 GPa), SnF<sub>2</sub> (55.60 GPa) and Li<sub>3</sub>PO<sub>4</sub> (10 GPa), the formation of Li dendrites is not fully eliminated, implying that any cracks in the protective layers or existing grain boundaries will become the defects allowing the dendrite penetration [12-14]. Therefore, from a different perspective, increasing the flexibility of the protective films has shown the potential to accommodate the extreme volume deformation of Li [15]. Meanwhile, building a stable protective film that can fundamentally prevent the formation of Li dendrites, in addition to providing mechanical suppression, is an attractive approach in the hope of terminating the safety hazards of Li metal batteries (LMBs) [16,17].

<sup>\*</sup> Corresponding authors.

It is known that the nucleation of Li dendrites is a result of nonuniform deposition of Li-ion flux in the electrolyte [18], because both Li ions and counterions are prone to diffuse near the pores of the separator. In this scenario, a dense and ion conductive protective film is expected to improve the overall uniformity of the ion fluxes [2,19–21]. Yet the migration of anions across the protective film still leads to the anion depletion on the anode surface and a gradually amplified electric field. This is the origin that drives the formation of Li dendrites according to the model proposed by Brissot and Chazalviel [22], which results in the breakage of SEI layers and poses safety risks again. Based on these considerations, one can anticipate that a protective film capable of anchoring anions and accommodating the dynamic Li deformation in cyclic processes is highly desired [23].

Proteins possess complex spatial structures and abundant functional groups such as -COOH, -OH, and  $-\text{NH}_2$  groups from the various amino acids [24]. Appropriate denaturation process can disrupt the inter-/intra-chain interactions and then expose the functional groups on the surface, which is a key step to functionalize proteins [25]. This feature makes proteins desirable and adaptive functional materials applicable in a variety of battery components. A number of studies on applying proteins as carbon source [26–28], binders [29–31], electrolytes [32,33], separator coatings [34–36], were reported. To the best of the authors' knowledge, however, the study on exploiting protein-derived, stretchable polymeric protective film for Li anode was rarely reported.

Here, taking a better utilization of the molecular interactions of zein (corn protein) via sustaining its denatured structures, we first time report a highly flexible and multifunctional polymeric protective film. The protein-enabled protective film, showing unique selfadapting and anion-anchoring functions, is fabricated by incorporating denatured protein with polyethylene oxide (PEO) as an agent for suppressing the protein refolding via forming good miscibility and intermolecular bonding between them. Therefore, the protein-enabled protective film with excellent flexibility, strong adhesion strength, and anion-anchoring ability is obtained, which not only adapts and regulates the interface but also stabilizes the Li-ion flux. As a result, the Li anode protected by the selfadapting and anion-anchoring protective film delivers stable plating/stripping process for more than 500 h. Coupling the protective film with Li<sub>2</sub>MnO<sub>4</sub> cathode, the capacity and cycle stability are significantly improved as well.

# 2. Experimental

# 2.1. Fabrication of polymeric films

The preparation of all the solutions and polymeric films was performed in an Ar-filled glovebox with both water and oxygen content less than 0.5 ppm. The remnant moisture in the solvents was removed by molecular sieve. Li metal was gently polished by a toothbrush with hexane in the glovebox prior to use. To prepare the zein@PEO film, 0.5 wt% PEO (M.W. = 5 million g mol<sup>-1</sup>) and 0.25 wt% zein (Sigma Aldrich) were dissolved in dimethyl sulfoxide (DMSO) under stirring at 50 °C for 24 h. Thereafter, 10  $\mu$ L of the asprepared solution was dipped on the polished Li surface and dried at 50 °C for 10 h. To prepare PEO or zein films, the solutions were 0.5 wt% PEO or 0.5 wt% zein dissolved in DMSO and the solutions were dipped on Li using the same procedures above. To study the properties of the polymer films in a battery, the films were plasticized by certain amount (e.g., weight ratio of film: electrolyte = 1:5) of liquid electrolyte. The composition of the added liquid electrolyte is 1 M lithium bis(trifluoromethane sulfonyl) imide (LiTFSI) in the solution of 1,3-dioxolane (DOL) and 1,2dimethoxyethane (DME) with 1 wt% LiNO<sub>3</sub>. The electrolyte solvents were totally removed by drying in a vacuum oven at 50 °C for 48 h. The remaining solid samples were designated as PEO-Li<sup>+</sup>, zein-Li<sup>+</sup> and zein@PEO-Li<sup>+</sup>, respectively.

#### 2.2. Materials characterization

Due to the poor stability of Li metal in ambient atmosphere, the polymer films of PEO, zein and zein@PEO were characterized individually. Scanning electron microscopy (SEM, Quanta 200F) was used to characterize the morphology of pristine and cycled Li metals. To obtain the surface roughness of the cycled Li metal anodes, an optical digital microscope (KEYENCE VHX-7000) was used with varying focus positions to gain the 3D measurement on the surface roughness. It is noted that the cycled Li metals were fully rinsed by DOL/DME solvent before morphology observation. Fouriertransform infrared spectroscopy (FTIR, Thermofisher iS10) was applied to investigate the interactions among PEO, zein and Li salt using an ATR mode. The mechanical properties were measured by a dynamic mechanical analyzer (DMA, 0800) using a tensile mode with a strain rate of 5% min<sup>-1</sup>. The thermal properties of the films were investigated by Differential scanning calorimetry (DSC, Mettler Toledo) with a heating rate of 5 °C min<sup>-1</sup>. The adhesion strength of three films on Cu and Al foils and their rheological properties were measured by using a rheometer (HR-2, TA Instruments). For the adhesion strength testing, a 3 M tape was adhered to the film sample (effective area: 1 cm  $\times$  1.5 cm), which was attached to the rheometer sample holder. The other side of the tape was lifted by the steel tip of the rheometer with a constant speed of 50  $\mu m \ s^{-1}$ . The axial force (peeling force) against time was recorded in this process. The rheological properties were obtained using a frequency sweep mode from 0.1 to 100 Hz with a controlled stain of 1% at room temperature.

## 2.3. Electrochemical characterization

Li/Cu cell. All of the electrochemical performance of the Li anodes was tested in CR-2032 coin type cell. Li/Cu cells were assembled in an Ar-filled glovebox ( $H_2O < 0.5$  ppm,  $O_2 < 0.5$  pp m). The electrolyte amount of Li/Cu cells was controlled to be 40  $\mu$ L [37]. The voltage of Li/Cu cell was set from -0.5 to 0.5 V, applying various current densities of 0.4 and 0.8 mA cm<sup>-2</sup> with a constant capacity (0.8 mAh cm<sup>-2</sup>). The rate performances of Li/Cu cell based on zein@PEO modified Li and pristine Li anode were further measured in higher current densities of 1.2, 1.6, 2, 2.4, 2.8, 3.2, 3.6, 4 mA cm<sup>-2</sup> with a constant capacity of 0.8 mAh cm<sup>-2</sup>. The impedance of Li/Cu cells was characterized by electrochemical impedance spectroscopy (EIS) with a frequency range of 0.01–10<sup>6</sup> Hz by electrochemical workstation (Biologic VSP EC-Lab).

Li/LiMn<sub>2</sub>O<sub>4</sub> half-cell. LiMn<sub>2</sub>O<sub>4</sub> cathode electrodes were prepared by casting a slurry of LiMn<sub>2</sub>O<sub>4</sub> (MTI Corp.), carbon black (SuperC45, MIT Corp.) and polyvinylidene fluoride (PVDF) with a weight ratio of 90:5:5 in *N*-methyl-2-pyrrolidone (NMP) solvent onto a carbon-coated Al foil and transferred into a vacuum oven at 60 °C for 12 h. Then, the dried cathode sheet with an active material loading of 5.25 mg cm<sup>-2</sup> was cut into small discs with a diameter of 12.7 mm. The electrolyte for Li/LiMn<sub>2</sub>O<sub>4</sub> cell is composed of ethylene carbonate (EC) and diethyl carbonate (DEC) (volume ratio of EC:EMC = 1:1) with 1 M LiPF<sub>6</sub>. The electrolyte amount was controlled to be 40  $\mu$ L. The cycle voltage range of Li/LiMn<sub>2</sub>O<sub>4</sub> cells was 3.0–4.3 V.

# 3. Results and discussion

Our previous studies [38,39] indicated that protein showed unique interactions with electrolyte ions, particularly anions,

owing to the positively charged amino acids (Lys., Arg., etc.) in the protein structure. Thus, utilizing protein to fabricate a welldesigned protective film is favorable to stabilize the ion deposition and diminish the possibility of dendrite formation. However, the inherent refolding of denatured protein chains leads to the structural fracture and buries the functional groups again. Therefore, as depicted in Fig. 1(a), we rationally incorporated PEO into this system to suppress the chain refolding from the denatured zein, due to their high miscibility and intermolecular bonding, which will be discussed in the present study. Transforming the generated zein@PEO layer to a protective film for Li anode is expected to help the anchoring of anions for stabilizing the deposition of Li-ion flux in Fig. 1(b). In addition to this benefit, we note that although PEO is a favorable ion conductor, it suffers from inferior mechanical properties when swelling in the liquid electrolyte [40], such that the addition of rigid protein effectively improves its mechanical performance. Meanwhile, the rich functional groups from the amino acids of zein may also provide various interactions with substrates, which is anticipated to strengthen the adhesion to Li metal. As a result, the rational combination of zein and PEO synergistically

generates a highly flexible, conformable and anion-anchoring protective film that can well stabilize the Li metal.

As illustrated in Fig. 1(c), the protein-enabled protective film (zein@PEO) was fabricated by simply casting the solution on Li metal. Benefiting from the significant properties including ionredistribution ability, high flexibility, and good adhesion, the zein@PEO protective film demonstrates an evident effectiveness in stabilization of Li deposition and adapting with the huge volume change of Li. For a pristine Li in Fig. 1(d), the intrinsically imperfect surface of Li and uneven distribution of Li-ion flux generate a "tip effect", in which the current density tends to increase than elsewhere. These "tips" become the preferable sites for Li deposition, thereafter, driving the growth of Li dendrites [16]. Meanwhile, the subsequent Li plating process causes an extreme volume expansion, which may break the SEI layer due to the stress increase. In the following stripping process, Li dendrites may shrink or fracture, making fresh Li exposed, SEI laver broken and "dead" Li formation [1]. To solve these issues, a highly flexible and adhesive protective film that can redistribute the Li-ion flux and conformably adapt with the volume change is proposed in

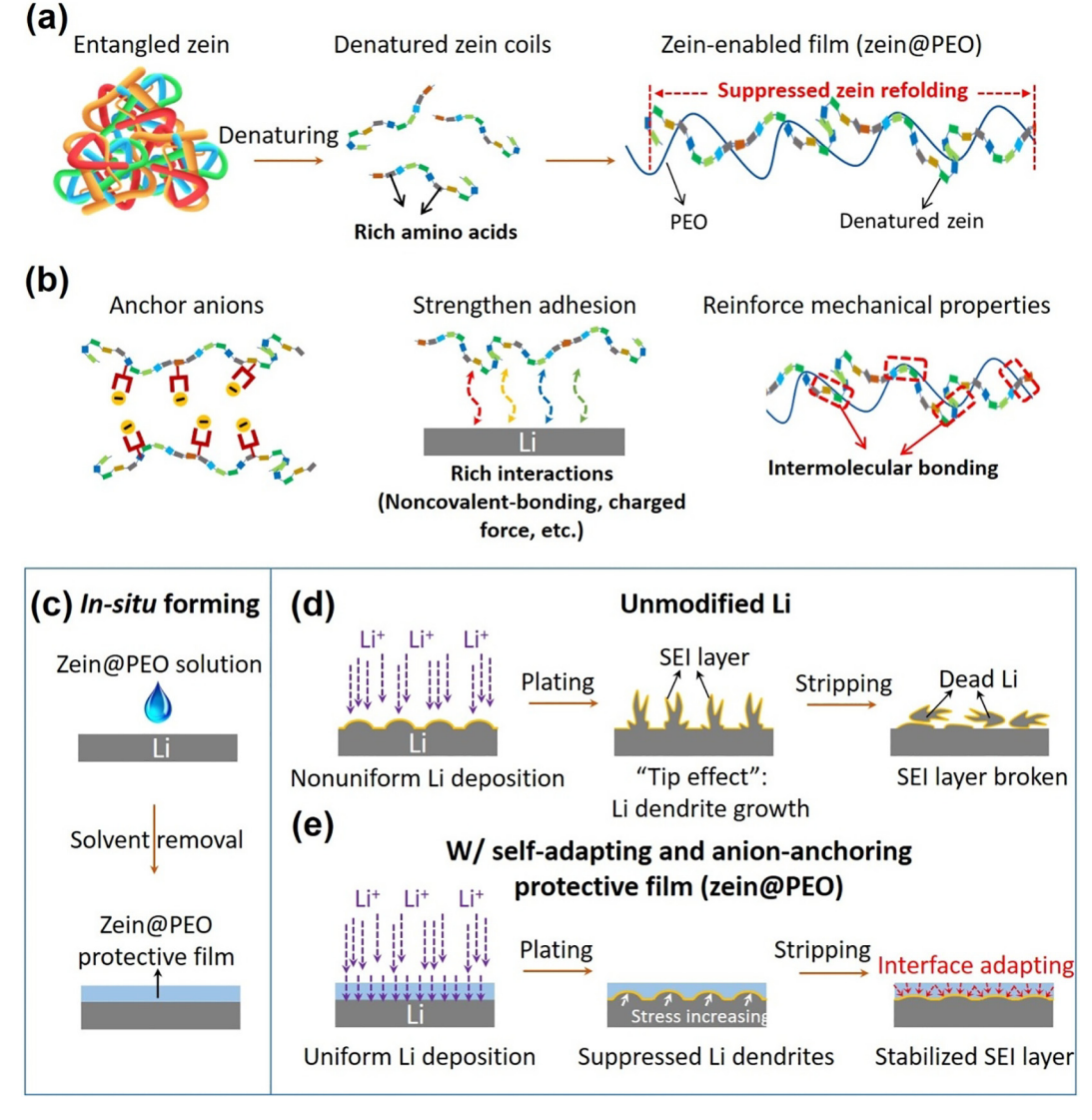


Fig. 1. Design concept, schematic illustration of fabrication process of the protein-enabled protective film, and the comparison of Li plating/stripping behaviors. (a) Schematic of the denaturation of zein protein to expose its functional groups and fabrication of the zein-enabled protective film (zein@PEO). (b) Contributions from zein to the significant properties of the zein@PEO protective film. (c) Modification of Li metal via in-situ forming zein@PEO protective film on the surface. Schematics of the Li plating/stripping behaviors for (d) pristine Li and (e) Li modified by the PEO/protein protective film.

Fig. 1(e). As shown, the zein@PEO protective film possesses a high flexibility, strong adhesion to the Li surface, ion-conduction ability, as well as a certain anchoring effect for the anions in the electrolyte. The zein@PEO protective film acts as a buffering layer to redistribute the originally uneven ion flux, and more importantly, to increase more the uniformity of the Li-ion flux due to the limited movement of anions. During the repetitive plating/stripping processes, the high adhesion of zein@PEO protective film provides strong binding with the Li metal [41]; the exceptional flexibility has a positive effect on accommodating the volume deformation of Li. The stress increase from the Li plating can be adapted by the zein@PEO protective film due to the strain variation, thus stabilizing the Li-SEI interface. As a result, the zein@PEO protective film effectively homogenizes the ion deposition and affords the volume change, while protects the Li metal from the parasite interaction with electrolytes.

We first studied the morphologies of various polymer films that were in-situ formed on the Li metal. As shown in Fig. 2(a) (see more cross-sectional SEM images in Fig. S1a and b), the PEO film exhibits a smooth and dense surface due to its good film forming property, which shows a thickness of ca. 1.24 µm in Fig. S2(a). However, many cracks are present in the zein film, because the zein coils are prone to re-entangle or refolding during the solvent removal process driven by their strong inter-/intra-chain interactions [42]. The rigidity of protein is also a factor generating the cracks. These fractures on the Li surface will become the defects that more severely deteriorate the homogeneity of ion deposition [43]. Incorporating PEO with zein yields a uniform and crack-free film, due to the good PEO-zein miscibility by the intermolecular interaction that will be discussed in detail below. The film also shows no obvious zein aggregates (see more cross-sectional SEM images in Fig. S1e and f), indicating that the refolding of zein chains is depressed by PEO. The thickness of the zein@PEO film is ca. 2.56 μm as indicated by the cross-sectional SEM image in Fig. S2(c).

The intermolecular interactions among the film components were investigated by FTIR (Fourier-transform infrared spec-

troscopy). As shown in Fig. 2(b), the PEO film shows two characteristic peaks at 1100 and 840 cm<sup>-1</sup>, ascribed to the antisymmetric stretching of C-O-C and wagging of CH<sub>2</sub>, respectively [44]. The two peaks of zein located at 1645 and 1537 cm<sup>-1</sup> correspond to C = O stretching (amide I) and N-H bending (amide II), respectively [45]. Regarding the zein@PEO blend, the characteristic peaks of both PEO and zein are observed. One finds a noticeable red shift for both  $C = O(1652 \text{ cm}^{-1})$  and  $N-H(1541 \text{ cm}^{-1})$  groups, indicating the formation of H-bonding between them as illustrated in Fig. 2(c) [46]. This is the primary reason for the good miscibility between PEO and zein, and the H-bonding is favorable for physically linking the two polymers and improving the mechanical properties. In fact, the polymeric protective film in a battery adsorbs a copious amount of liquid electrolyte, meaning that the Li salt will also be adsorbed and complex with the polymers such as PEO. We thus investigated the interactions among PEO. zein and Li salt by introducing LiTFSI in the polymer films. As shown in Fig. 2(d), the C-O-C peak of PEO, originally located at 1100 cm<sup>-1</sup> (Fig. 2b), is significantly less intense. This is due to the coordination between Li<sup>+</sup> and the ether oxygen atom of PEO, which is consistent with the previous reports [47]. Interestingly, for the zein-Li<sup>+</sup> system, there is a notable blue shift for both C-SO<sub>2</sub>-N (from 1132 to 1144 cm<sup>-1</sup>) and C-F (from 1184 to 1199 cm<sup>-1</sup>) [48], which suggests that zein may generate some interaction with the TFSI- anion, most likely electrostatic interaction from the positively charged amino acid groups (e.g., Arg., Lys. His).

The thermal and crystallization behaviors of the polymer films were investigated using differential scanning calorimeter (DSC). As shown in Fig. 3(a), the two endothermic peaks of PEO and zein@PEO films are ascribed to the melting of crystals [49]; zein has no significant melting behavior in the temperature range due to its amorphous nature after denaturation. Specifically, the melting point ( $T_{\rm m}$ ) of zein@PEO (65 °C) shifts to a lower value compared with PEO (67 °C), which indicates that the introduction of zein intervenes the chain regularity of PEO by forming H-bonding as

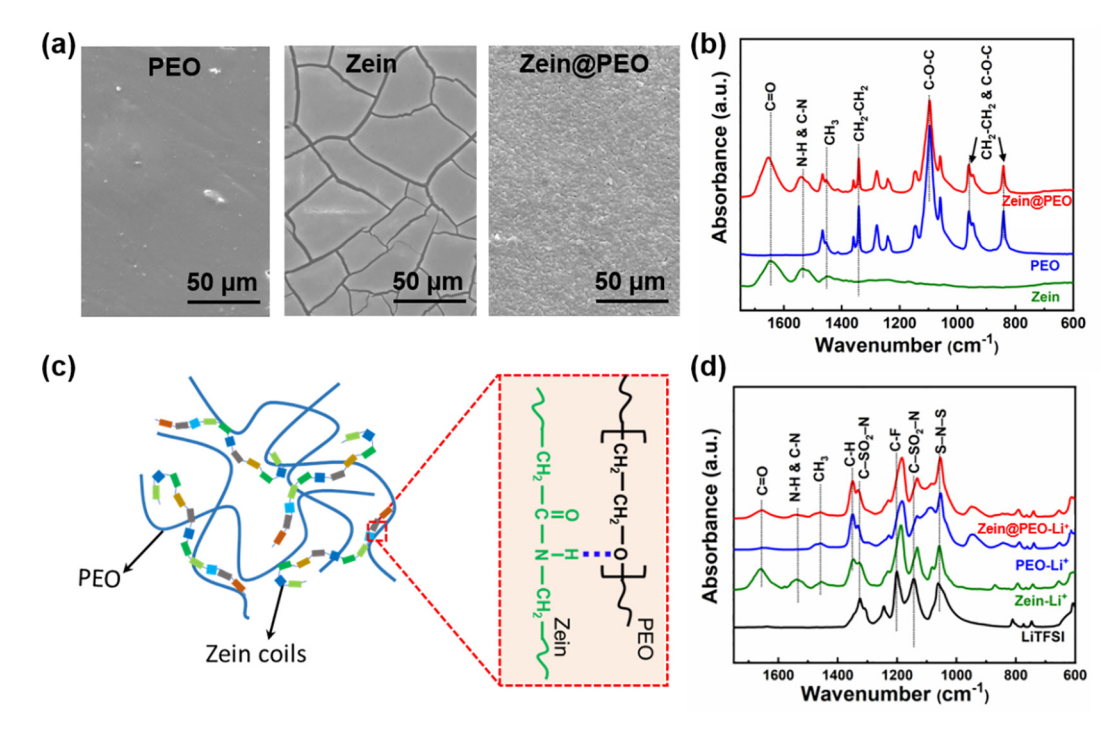


Fig. 2. Morphological studies of various polymer films. (a) SEM images of PEO, zein and zein@PEO films in-situ deposited on Li metal, respectively. (b) FTIR spectra of various polymer films. (c) Schematic of the H-bonding formation between PEO and zein. (d) FTIR spectra of polymer-Li\* complex films.

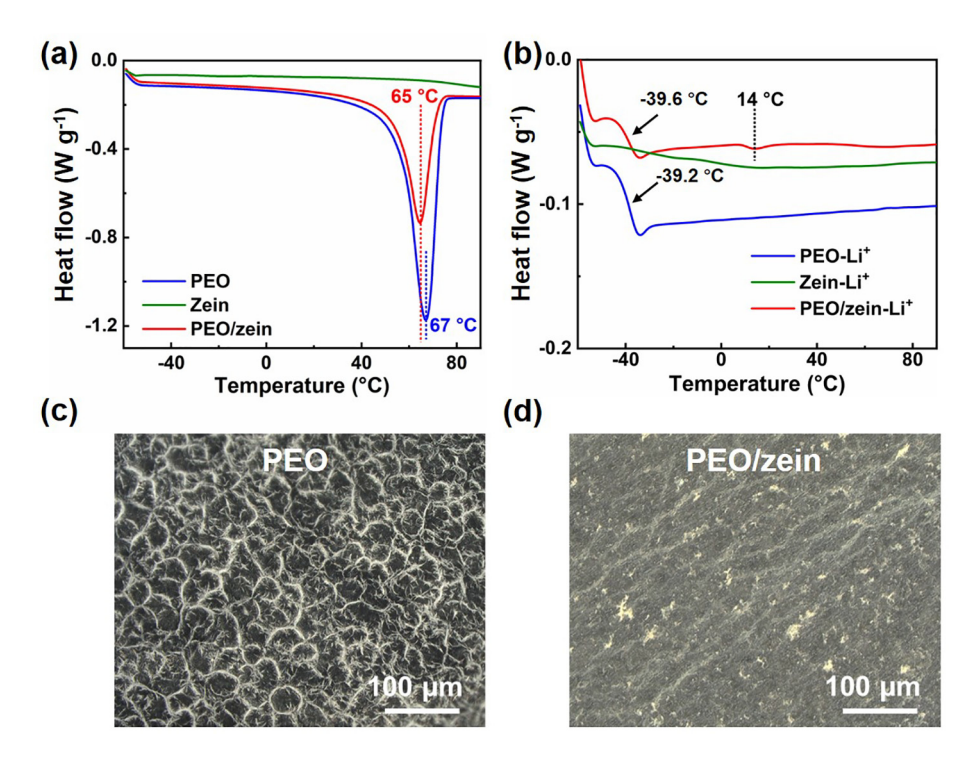


Fig. 3. Thermal properties and crystallization behaviors of various polymer films. DSC curves of various (a) polymer films and (b) polymer-Li\* films. Polarized optical microscopy images of (c) PEO and (d) zein@PEO films, respectively.

discussed above. This also decreases the possibility of crystalline phase formation of PEO. Furthermore, when adding a proper loading of LiTFSI to the polymers (53 wt%), the crystallization of PEO is completely depressed, indicated by the absent melting peaks of both PEO-Li<sup>+</sup> and zein@PEO-Li<sup>+</sup> blend (Fig. 3b). This is a combined result of the Li<sup>+</sup>-O coordination interaction and the severe entanglement of the ultrahigh molecular weight PEO chains. The amorphous ultrahigh molecular weight PEO-Li<sup>+</sup> complex is favorable for increasing the adhesion strength, which was reported by our previous study [50] and is critical for yielding an adaptive and conformable protective film. There is a new endothermic shoulder at 14 °C for zein@PEO-Li<sup>+</sup> film, which might be attributed to the intermolecular bonding between PEO and zein. Both PEO-Li<sup>+</sup> and zein@PEO-Li<sup>+</sup> films show a single glass transition temperature  $(T_g)$ , which is -39.2 and -39.6 °C, respectively. Despite that the  $T_{\sigma}$  of zein was reported to be ~150 °C [51], zein shows no obvious  $T_{\rm g}$  in this temperate range from our study. Thus, to further understand the miscibility between PEO and zein, we characterized the crystalline morphologies of PEO and zein@PEO films using polarized optical microscopy in Fig. 3(c and d). As shown, PEO exhibits a significant number of crystals due to its semi-crystalline structure. The addition of zein substantially changes the morphology of PEO. There is no phase separation for the zein@PEO film, and the crystal morphology of PEO is obviously changed, which is possibly due to the heterogeneous nucleation from zein particles in Fig. 3(d). These results indicate a good miscibility between PEO and zein, which benefits the enhancement in adhesion and mechanical properties as will be discussed below.

The adhesion strength of protective film with Li metal is a significant property that has a notable impact on the interface stability and adapting ability during volume deformation. As shown in Fig. S3, an adhesive tape is tightly adhered to the zein@PEO film and quickly peeled off from the Li metal. Then the remaining Li metal is taken out of the glove box and exposed to air. Compared with pristine Li darkening after exposure to air for 5 min, the color of Li with zein@PEO film is shinier. This demonstration indicates

that the zein@PEO film is not totally removed by the tape, indicating the residual of the film keeps the Li metal from corrosion. Therefore, the zein@PEO film shows certain adhesion with Li metal. Due to the instability of Li metal in ambient atmosphere, we further studied the detailed adhesion properties of the polymer films against aluminum (Al) and copper (Cu) metal substrates to mimic the binding behavior against Li. We find that the amorphous PEO-Li<sup>+</sup> and zein@PEO-Li<sup>+</sup> films exhibit good adhesion to both Cu and Al substrates as demonstrated in Fig. 4(a). However, the zein film easily delaminates from the metal substrate. These results suggest that the adhesion is mainly contributed by the amorphous PEO-Li<sup>+</sup> complex, in agreement with our previous studies. Fig. 4(b) shows the peeling force of PEO-Li<sup>+</sup> and zein@PEO-Li<sup>+</sup> films from the Cu substrate. It can be seen that the zein@PEO-Li<sup>+</sup> film shows a significantly higher peeling force (ca. 2.3 N) than that of the PEO-Li<sup>+</sup> film (ca. 0.75 N), implying a stronger adhesion strength to the Cu substrate. The enhanced adhesion property is contributed by the rich functional groups of zein, which adds more interactions with the substrate such as H-bonding, van der Waals force and electrostatic forces [41].

Fig. 4(c and d) presents the mechanical properties of the various polymer films by tensile testing. We first studied the polymer films without addition of Li salt so as to reveal the contribution from zein. As displayed in Fig. 4(c), the zein film shows a high Young's modulus of 0.86 GPa and a high yield strength of 2.33 GPa yet a minimal elongation due to its brittle nature. On the contrary, PEO and zein@PEO films undergo typical plastic deformation, and the addition of zein increases the mechanical performance of the film. The Young's modulus of the zein@PEO film is 0.63 GPa, which is much higher than that of the PEO film (0.39 GPa). The ultimate tensile strength of the zein@PEO film is increased to 1.45 GPa by zein, compared with that of the PEO film (1.29 GPa). Both PEO and zein@PEO films present notably higher elongation than that of the zein film. Specifically, the ultimate elongation (elongation at rupture point) of PEO and zein@PEO films is 78.3% and 75.1%, respectively. In a word, the addition of zein increases the tensile

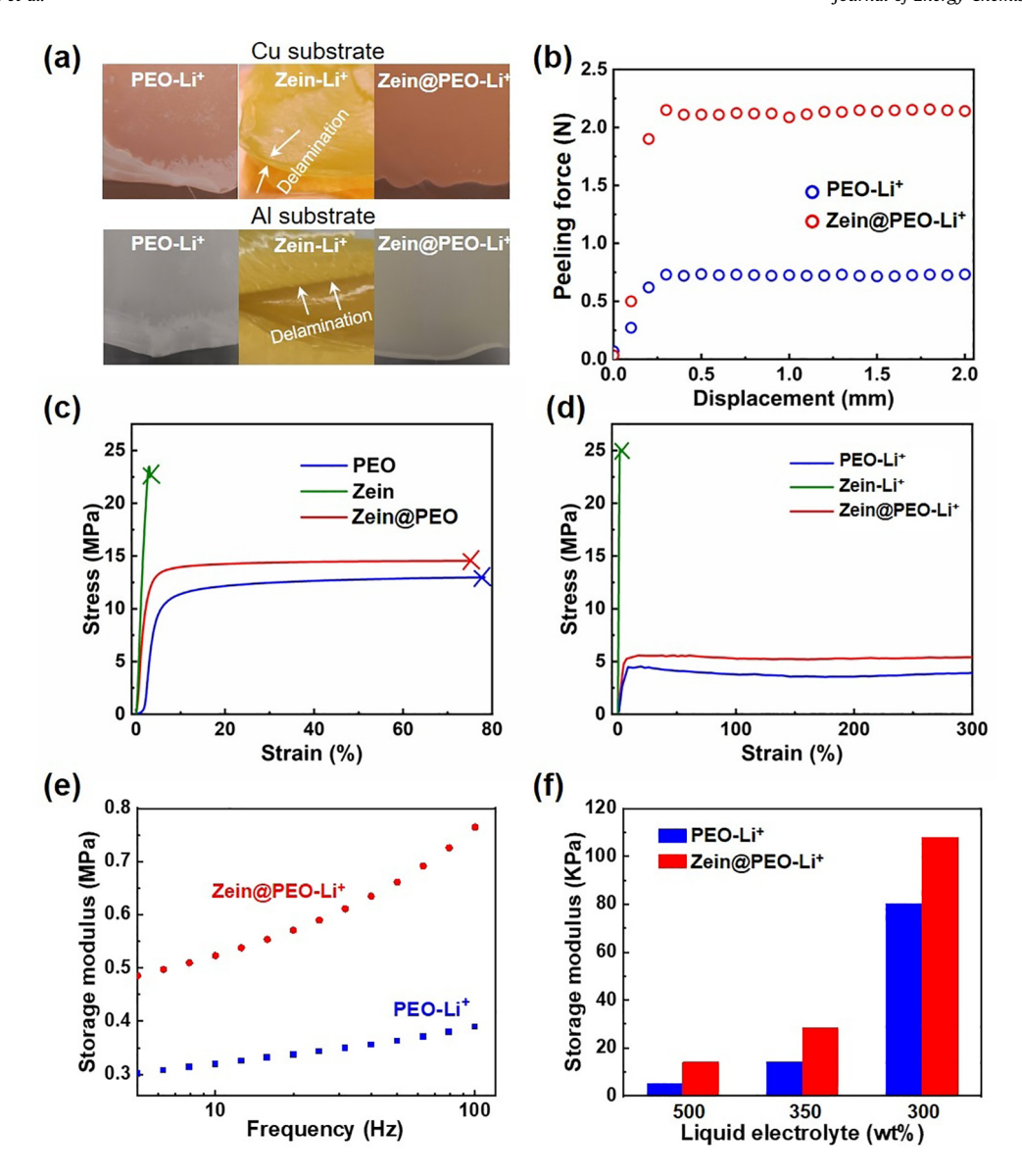


**Fig. 4.** Mechanical and adhesion properties of polymer films. (a) Photographs showing the adhesion behaviors of polymer films on Cu and Al foils. (b) Peeling force vs. displacement of the polymer films from Cu foil (peel speed = 50 μm min<sup>-1</sup>). Stress–strain curves of (c) polymer films and (d) polymer-Li\* films. (e) Frequency-dependent behaviors of the storage modulus of polymer-Li\* films. (f) Storage modulus of polymer-Li\* films with varying mass loading of liquid electrolytes.

strength and Young's modulus but slightly deteriorates the elongation compared with the PEO film. Interestingly, introduction of LiTFSI that induces an amorphous PEO system as discussed in Fig. 3(b), generates significantly improved flexibility in Fig. 4(d). In terms of the polymer films complexing with LiTFSI, we observe that the mechanical performance of zein shows no obvious change. However, it is worth noting that the PEO-Li<sup>+</sup> and zein@PEO-Li<sup>+</sup> films show exceptional flexibility. The elongation of both films is improved to be above 300%, while the Young's moduli are 0.5 and 0.7 MPa for PEO-Li<sup>+</sup> and zein@PEO-Li<sup>+</sup> films, respectively.

In addition, we soaked the PEO, zein and zein@PEO films in a liquid electrolyte solution (1 M LiTFSI in EC:EMC = 1:1 by volume) for various hours to study their swelling behavior. As shown in Fig. S4, the PEO film is almost dissolved by the liquid electrolyte after 24 h, which is consistent with previous work [52]. However, zein and zein@PEO maintain their film structure. Zein does not swell in a liquid electrolyte, such that the zein@PEO film becomes more resistant to dissolving by the liquid electrolyte in the presence of zein. This helps retain the mechanical performance of the zein@PEO film in a battery enriched with liquid electrolytes. To

elucidate the advantage of the zein@PEO film after being plasticized by the liquid electrolyte, we further studied the rheological properties of the swelling polymer films. Zein is not plasticized by the liquid electrolyte and still a rigid film after electrolyte treatment; therefore, the rheological measurement is not applicable. As shown in Fig. 4(e), the storage moduli of both plasticized films (500 wt% liquid electrolyte loading) are dependent on the frequency, indicating a typical viscoelastic behavior. Importantly, the storage modulus of the zein@PEO-Li<sup>+</sup> film is greatly higher than that of the PEO-Li<sup>+</sup> film. For instance, at a frequency of 100 Hz, the storage modulus of the zein@PEO-Li<sup>+</sup> film is 0.77 MPa, which is about twice that of the PEO-Li<sup>+</sup> film (0.38 MPa). Fig. 4(f) shows the storage moduli of the two films with varying loadings of the liquid electrolyte with respect to the film mass. It can be seen that decreasing the liquid electrolyte from 500 to 300 wt%, the storage moduli for both samples notably improve. The zein@PEO-Li+ film shows higher storage moduli than that of the PEO-Li<sup>+</sup> film throughout the measurement range. The above findings indicate that the addition of zein is critical to enhance the mechanical properties of the films in all the states: with or without Li salt/liquid electrolyte.

Therefore, the zein@PEO film integrates the advantages of flexibility, adhesion, and durability, making it an excellent protective film. In addition, due to the rich H-bonding, the zein@PEO film shows self-healing property, which helps maintain the structural integrity of the film during the repeated Li plating/stripping process. As shown in Fig. S5, the zein@PEO film is first plasticized by liquid electrolytes, and then cut into two pieces. After standing for about 1 min, the fracture gradually diminishes and the two broken parts merge together to the original state after 5 min.

The ion-transfer process leaves a space-charge region, which drives the growth of Li dendrites, such that immobilizing anions

can reduce the electric field intensity and delay the formation of Li dendrites [53]. In other words, increasing the Li-ion transference number is conducive to suppress the nucleation of Li dendrites. We measured the Li-ion transference number of the Li/Li symmetric cells with or without the zein@PEO protective film using a chronoamperometry method. From the initial and steady currents in Fig. 5(a), the zein@PEO film shows a much higher Li-ion transference number of 0.80, compared with the pristine Li cell (0.59). We attribute the improvement to the specific interactions between zein and ions. Zein is composed of 16 types of amino acids, among which the majority is glutamine, leucine, proline, alanine, pheny-

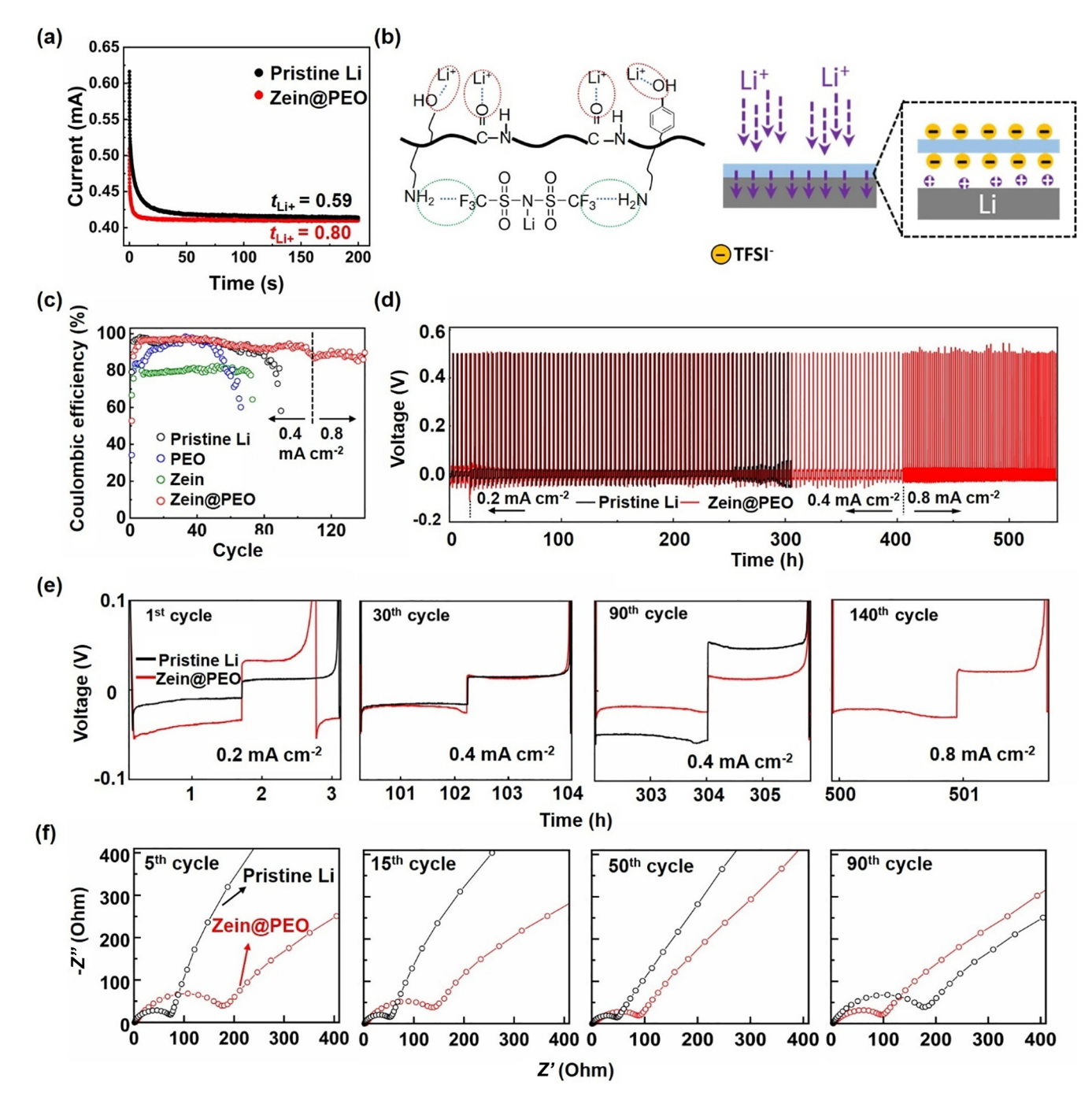


**Fig. 5.** Li plating/stripping behaviors based on Li/Cu cells. (a) Chronoamperometric plots obtained from symmetric Li cells. (b) Schematic of the contribution of zein to anchoring anions and then stabilizing ion deposition. (c) Coulombic efficiency of Li/Cu cells with different protective films at various current densities. (d) Galvanostatic cycling of Li/Cu cells with or without a zein@PEO protective film. (e) Voltage profiles extracted from the 1st, 30th, 90th, and 140th cycles. (f) Nyquist plots of Li/Cu cells after being operated for specific cycles (frequency range: 0.01–1 MHz).

lalanine and serine (Table S1). The polypeptide chains derived from these amino acids have peptide bond (-CO-NH-) on the backbone and abundant polar functional groups ( $NH_2$ , -OH, etc.) on the branch. In specific, -OH and C = O are lithiophilic groups, while  $-NH_2$  is anionphilic group (Fig. 5b) [54].

To reveal the effects of the various polymer films on the Li metal stabilization, the plating and stripping behavior of Li was investigated using Li/Cu cells with constant liquid electrolyte loading of 40 μL. The Coulombic efficiency of all cells is shown in Fig. 5(c), which is a key factor that reflects the stabilities for Li plating/stripping process and the protective film. The decay of Coulombic efficiency is a result of the consumption of Li and electrolytes by continuous Li-electrolyte side reactions. The initial Coulombic efficiencies are 79.15% (pristine Li), 66.67% (zein), 34.16% (PEO) and 52.7% (zein@PEO). The relatively low Coulombic efficiency is because of the reaction between the electrolyte and the passivation layer originally on the Li metal. It is noted that the PEO and zein@-PEO cells have much lower Coulombic efficiency than the pristine Li cell. This is possible because the DMSO treatment generates more passivation layer on the Li surface in the beginning, the dissolution of which consumes more Li source as confirmed in Figs. S6 and S7. Specifically, the DMSO treated Li anode experiences a lower Coulombic efficiency in the first couple of cycles, and then the efficiency increases gradually in the subsequent cycles in Fig. S7. Along with the cycling process, the Coulombic efficiency of all samples increases and gradually stabilizes. As shown, the Li anode modified by the zein film exhibits the lowest average Coulombic efficiency of 80% throughout the cycling process. This is because zein is not plasticized by the liquid electrolyte as revealed above (Fig. 4), leading to high resistance for ion-transfer. It is worth noting that the zein@PEO cell delivers a significantly higher Coulombic efficiency (93%) after cycling at 0.4 mA cm<sup>-2</sup> for 100 cycles, compared with the cells with pristine Li (<60% at the 90th cycle), PEO (<60% at the 66th cycle) and zein (ca. 80% at the 75th cycle). Even at a high rate of 0.8 mA g<sup>-1</sup>, the Coulombic efficiency of the zein@PEO cell keeps higher than 85% from the 105th to the 160th cycle. It is known that DMSO solvent can passivate the Li metal [55]. To study the impact from the DMSO solvent, we analyze the morphology of the Li metal treated by pure DMSO. In Fig. S6, it can be seen that a passivation layer is generated on the Li surface. In addition, we test the Coulombic efficiency of Li/Cu cells with DMSO treated Li and pristine Li in Fig. S7. As shown, the Coulombic efficiencies of both Li anodes are very close, indicating that DMSO treatment has no significant impact on the electrochemical performance, although more in-depth studies are necessary to uncover the long-term effect. These findings demonstrate that the zein@PEO film can effectively guide and homogenize the deposition of Li-ions, which suppresses the formation of Li dendrites and "dead" Li species.

The rate performance of the cells was tested at various current densities with a constant capacity of 0.8 mAh cm<sup>-2</sup> and is shown in Fig. S8. The zein@PEO cell exhibits remarkable rate performance compared with the pristine Li cell. At a current density of 0.4 mA cm<sup>-2</sup>, the Coulombic efficiency of both cells is close to 97%. At higher current densities of 0.8, 1.2 and 1.6 mA cm<sup>-2</sup>, the Coulombic efficiency of the zein@PEO cell slightly decreases to about 94%, 91% and 90%, respectively, while the corresponding values of zein@PEO cells are about 90%, 80%, and 70%, respectively. Surprisingly, when improving the current density to 2–5.6 mA cm<sup>-2</sup>, the zein@PEO cell still delivers a higher and more stable Coulombic efficiency compared with the pristine Li cell.

Fig. 5(d) shows the voltage profiles of Li/Cu cells containing a zein@PEO layer compared with the unmodified Li metal. A constant capacity of 0.8 mAh cm $^{-2}$ Li was deposited with varying current densities of 0.2 (first 5 cycles), 0.4 (the 6th–110th cycles), and 0.8 mA cm $^{-2}$  (after the 110th cycles). The pristine Li cell shows a

drastically increased polarization from 250 h, indicating a significant consumption of electrolytes due to the repetitive broken/repair of SEI layer. In contrast, the cell with the zein@PEO film exhibits a stable voltage profile over 540 h even at an increased current density of 0.8 mA cm<sup>-2</sup>. To deeply understand the contributions from the zein@PEO film on the Li plating/stripping behavior, the voltage profiles of the 1st, 30th, 90th, and 140th cycles were enlarged and shown in Fig. 5(e). In the 1st cycle, the pristine Li cell shows a much smaller polarization (0.013 V) than that of the zein@PEO cell (0.048 V). This is because the additional zein@PEO layer induces extra resistance initially, and an activation process is necessary. Interestingly, the polarization of zein@PEO cell notably decreases to the comparative level of the pristine Li cell in the 30th cycle, and the plating/stripping voltage plateaus for both cells are smooth. Along with the subsequent cycling, one sees that the polarization of zein@PEO cell (0.014 V) is lower than that of the pristine Li cell (0.015 V). The plateau voltage of zein@PEO cell keeps unchanged from the 90th to 140th cycle. These results indicate that the zein@PEO layer ensures stable and smooth plating/ stripping of Li dynamically and avoids the side reactions between Li and electrolytes. To further study the interface evolution in the continuous Li plating/stripping process, electrochemical impedance spectroscopy (EIS) was performed on the Li/Cu cells upon specific cycles. The Nyquist plots obtained from the Li/Cu cells after 5 cycles at 0.2 mA cm $^{-2}$  and 15, 50, and 90 cycles at 0.4 mA cm $^{-2}$ are shown in Fig. 5(f). All the plots consist of a semicircle at intermediate frequency region and a line at low frequency region, which are correlated with the charge-transfer  $(R_{ct})$  process and solid-state diffusion (Warburg impedance, Z<sub>w</sub>) of Li-ions, respectively. For the zein@PEO cell, the slope of the straight lines in low frequency region decreases with the increase of cycling number. Whereas the slope of the cell with pristine Li keeps nearly unchanged during cycling. This comparison demonstrates that the interface layer has a swelling equilibrium with the electrolyte solution. Additionally, it is found that from the 5th-50th cycling period, the R<sub>ct</sub> of the zein@PEO cell is higher than that of the pristine Li cell, resulting from the extra resistance from the polymer film that increases the ion-transport distance. Yet we can find that the  $R_{ct}$  of both cells decreases with cycling, and the decreasing trend is more obvious for the zein@PEO cell (Table S2). In the 90th cycle, the zein@PEO cell exhibits a lower  $R_{ct}$  of 111  $\Omega$ , which keeps a negligible change from the 30th cycle. On the contrary, the pristine Li cell shows a notable increase to 191  $\Omega$  in the 90th cycle, due to the severe depletion of electrolytes in the long-term cycling process. These results verify our finding that the zein@PEO film, despite of its increase in ion-transport resistance, shows the effectiveness in stabilizing the deposition of Li-ion flux, and protecting the Li metal from parasite reactions.

The morphologies of the cycled Li anode (70 cycles) at plating state were further observed. In Fig. 6(a), the cycled pristine Li shows considerable dark "dead" Li particles, forming a rough surface with a broader range of thickness (Fig. 6b). Fig. 6(c) shows severe fractures on the surface (see more SEM images in Fig. S9), which is due to the breaking of SEI layers and the formation of "dead" Li species. The cross-sectional SEM image in Fig. 6(d) further confirms the thick and broken "dead" Li layer. In contrast, the Li anode with the zein@PEO film forms a much smoother surface (Fig. 6e), showing a narrower roughness range of 0-10 μm (Fig. 6f) compared with the pristine Li. Importantly, it is shown a seamless zein@PEO coating on the Li surface in Fig. 6(g and h). The surface is dendrite-free and extremely homogeneous, and there are no noticeable "dead" Li species (also see SEM images in Fig. S10). These results are mainly due to the unique selfadapting behavior of the zein@PEO layer. The strong adhesion to the Li metal makes the zein@PEO layer firmly stick to the Li surface. During the volume shrinkage/expansion of Li, the exceptional

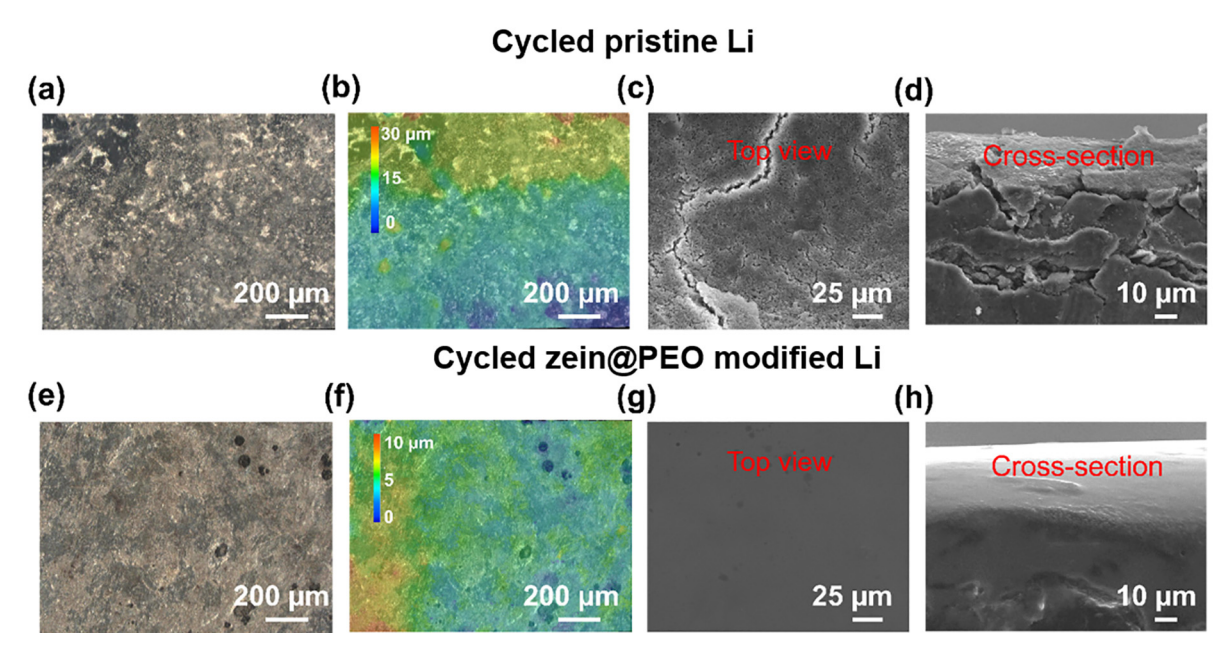


Fig. 6. Morphologies of cycled Li metal. (a) Optical microscopy image and (b) thickness analysis of the cycled pristine Li metal. (c and d) SEM images of the cycled pristine Li metal. (e) Optical microscopy image and (f) thickness analysis of the cycled Li metal with zein@PEO film. (g and h) SEM images of the cycled Li metal with zein@PEO film.

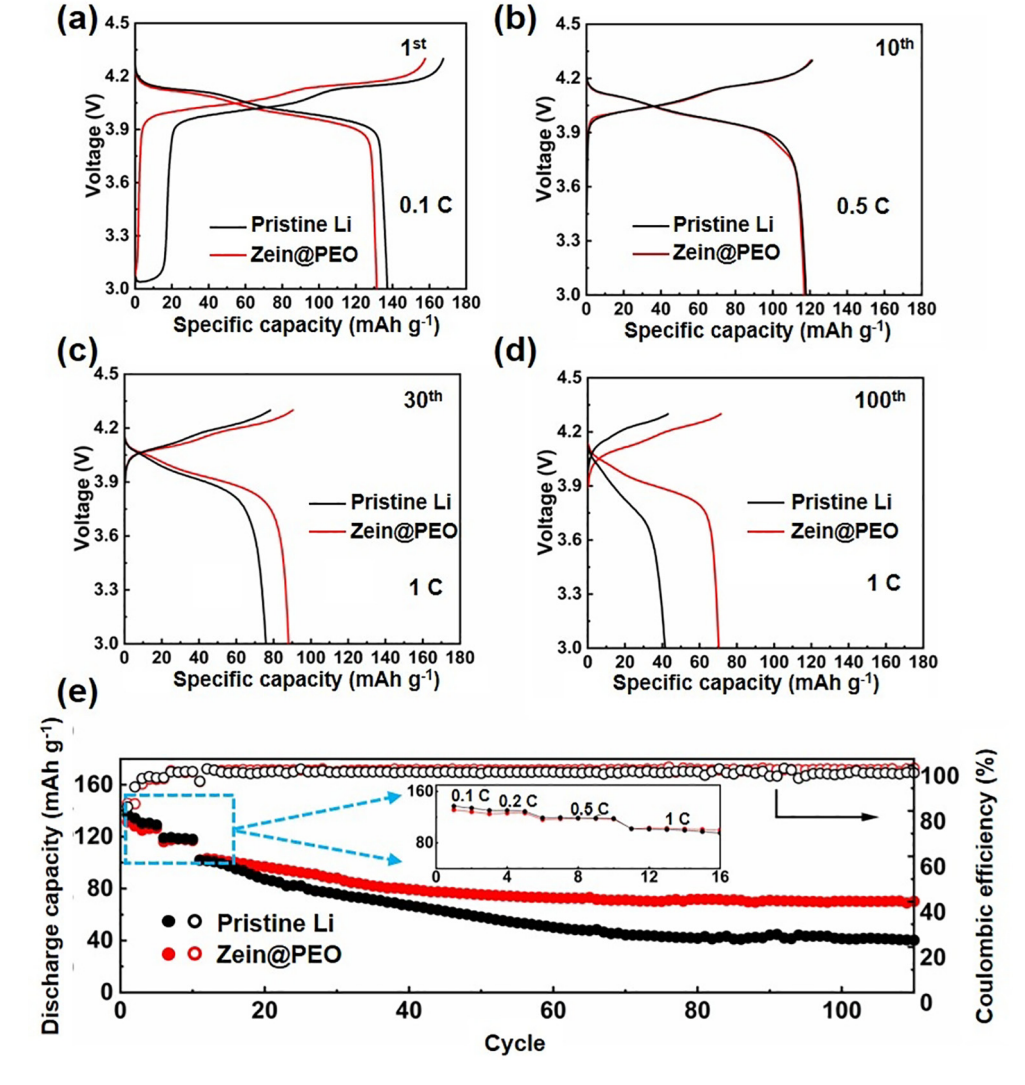


Fig. 7. Electrochemical performances of Li modified with zein@PEO film in Li/LiMn<sub>2</sub>O<sub>4</sub> half cells. (a)–(d) Charge-discharge profiles at the 1st, 10th, 30th, and 100th cycles, respectively. (e) Cycle and rate performances of the Li/LiMn<sub>2</sub>O<sub>4</sub> cells. The long-term performance was tested at 1 C.

flexibility allows the zein@PEO layer to adapt with the interface fluctuation by strain change without delaminating from the Li surface as illustrated in Fig. 1(c). Moreover, the ability for anchoring the anions further increases the stability and uniformity for the deposition of Li-ion flux. The synergistic effect finally contributes to the Li deposition in a dendrite-free way and protects the Li metal from side reactions.

To demonstrate the effectiveness of the zein@PEO film in stabilizing Li metal in a battery, the electrochemical performance of Li/ LiMn<sub>2</sub>O<sub>4</sub> cells was investigated. As shown in Fig. 7(a), in the initial cycle the zein@PEO cell yields a discharge capacity of 131.4 mAh g<sup>-1</sup>, which is slightly lower than that of the cell with pristine Li (137.1 mAh g<sup>-1</sup>). This is because for the fresh cell, the zein@PEO film on the Li metal is an inert layer without ion-conduction ability. Due to the plasticizing effect from the electrolyte, the zein@-PEO film becomes activated and ion-conductive with the cycling process. A small charge plateau at 3.07 V can be found for both cells, which is attributed to the de-lithiation process of the transformation from  $Li_xMn_2O_4$  (1 < x < 2) to  $LiMn_2O_4$  [56]. It is noted that the plateau (~3 V) of the cell with zein@PEO film is much shorter than the pristine Li cell. We speculate that some components from protein may accept the Li source from the excess Li of Li<sub>x</sub>Mn<sub>2</sub>O<sub>4</sub> [57]. In the 10th cycle at 0.5 C (Fig. 7b), the capacity of the zein@PEO cell overtakes the pristine Li cell, resulting from the activated zein@PEO film that is able to transport ions. At a high current rate of 1 C in Fig. 7(c and d), both cells exhibit typical LiMn<sub>2</sub>O<sub>4</sub> charge-discharge curves, demonstrating the reversible electrochemical reactions. Significantly, it is found that the cell with the zein@PEO film delivers notably higher capacities than that of the cell with pristine Li.

The cycle performances of both cells are shown in Fig. 7(e). The zein@PEO and pristine Li cells show discharge capacities of 131.4 and 137.1 mAh g $^{-1}$  in the first cycle, respectively. At 0.2 C, both cells deliver nearly the same capacity of ca. 118 mAh g $^{-1}$  (see the inset). The long-term cycle stability was investigated at 1 C. As shown, the zein@PEO cell shows much higher capacities compared with the pristine Li cell. In the 110th cycle, the capacity of zein@PEO cell is 70.2 mAh g $^{-1}$ , which is much higher than that of the cell with pristine Li (41.6 mAh g $^{-1}$ ). The capacity retention of zein@PEO and pristine Li cells are 53.4% and 29.3%, respectively (see Fig. S11). In addition, the Coulombic efficiency of the zein@PEO cell (>98%) is also higher than the counterpart (ca. 97%) from the 11th to 110th cycle. The above results are an evident indication that the zein@PEO film shows the potential to stabilize LMBs.

#### 4. Conclusions

In summary, we have reported a self-adapting and anionanchoring polymeric protective film for stabilizing LMBs. The protective film is fabricated by incorporating zein protein with PEO as an agent for restraining the protein refolding via forming good miscibility and intermolecular bonding between them. The resulting protein-enabled zein@PEO film synergistically integrates the advantages of excellent flexibility, strong adhesion and high Liion transference number (0.80). Thus, the zein@PEO protective film can accommodate the volume change and prevent the parasite interactions by forming a seamless coating on Li and adapting with the interface change. The ion-conduction ability and anionanchoring effect enable the zein@PEO film to redistribute and homogenize the Li-ion flux, fundamentally suppressing the formation of Li dendrites. As a result, the Li metal is effectively stabilized and protected by the zein@PEO film, and the lifespan of Li/Cu cells is prolonged to be more than 500 h. Coupled with LiMn<sub>2</sub>O<sub>4</sub> cathode, the zein@PEO film significantly improves the capacity, rate performance, and cycling stability compared with unmodified Li

metal. The reported flexible, adhesive and anion-immobilizing film design proposes a novel and promising strategy to solve the persistent issues in LMBs.

# **Declaration of Competing Interest**

The authors declare that they have no known competing financial interests or personal relationships that could have appeared to influence the work reported in this paper.

#### Acknowledgments

This work was supported by NSF CBET 1929236. The authors would like to gratefully acknowledge the support on microscopy characterizations from the Franceschi Microscopy & Imaging Center at Washington State University.

# Appendix A. Supplementary data

Supplementary data to this article can be found online at https://doi.org/10.1016/j.jechem.2021.05.014.

#### References

- [1] D. Lin, Y. Liu, Y. Cui, Nat. Nanotechnol. 12 (2017) 194-206.
- [2] J. Zheng, M.S. Kim, Z. Tu, S. Choudhury, T. Tang, L.A. Archer, Chem. Soc. Rev. 49 (2020) 2701–2750.
- [3] G. Yasin, M. Arif, T. Mehtab, X. Lu, D. Yu, N. Muhammad, M.T. Nazir, H. Song, Energy Storage Mater. 25 (2020) 644–678.
- [4] X. Gao, Y.N. Zhou, D. Han, J. Zhou, D. Zhou, W. Tang, J.B. Goodenough, Joule 4 (2020) 1864–1879.
- [5] Q. Zhang, S. Liu, Y. Lu, L. Xing, W. Li, J. Energy Chem. 58 (2021) 198-206.
- [6] R. Xu, X.Q. Zhang, X.B. Cheng, H.J. Peng, C.Z. Zhao, C. Yan, J.Q. Huang, Adv. Funct. Mater. 28 (2018) 1–7.
- [7] H.K. Jing, L.L. Kong, S. Liu, G.R. Li, X.P. Gao, J. Mater. Chem. A 3 (2015) 12213– 12219.
- [8] S. Choudhury, Z. Tu, S. Stalin, D. Vu, K. Fawole, D. Gunceler, R. Sundararaman, L. A. Archer, Angew. Chem. Int. Ed. 56 (2017) 13070–13077.
- [9] Y. Tang, L. Zhang, J. Chen, H. Sun, T. Yang, Q. Liu, Q. Huang, T. Zhu, J. Huang, Energy Environ. Sci. (2021) 602–642.
  [10] X. Shen, R. Zhang, X. Chen, X.B. Cheng, X. Li, Q. Zhang, Adv. Energy Mater. 10
- (2020) 1–8. [11] X. Liang, Q. Pang, I.R. Kochetkov, M.S. Sempere, H. Huang, X. Sun, L.F. Nazar,
- Nat. Energy 2 (2017) 1–7.
- [12] S. Li, L. Fan, Y. Lu, Energy Storage Mater. 18 (2019) 205-212.
- [13] R. Pathak, K. Chen, A. Gurung, K.M. Reza, B. Bahrami, J. Pokharel, A. Baniya, W. He, F. Wu, Y. Zhou, K. Xu, Q. (Quinn) Qiao, Nat. Commun. 11 (2020) 1–10.
- [14] N.W. Li, Y.X. Yin, C.P. Yang, Y.G. Guo, Adv. Mater. 28 (2016) 1853–1858.
- [15] G. Li, Y. Gao, X. He, Q. Huang, S. Chen, S.H. Kim, D. Wang, Nat. Commun. 8 (2017) 850.
- [16] Z. Luo, X. Qiu, C. Liu, S. Li, C. Wang, G. Zou, H. Hou, X. Ji, Nano Energy 79 (2021) 105507.
- [17] C. Yan, R. Xu, Y. Xiao, J.F. Ding, L. Xu, B.Q. Li, J.Q. Huang, Adv. Funct. Mater. 30 (2020) 1–21.
- [18] Y. Guo, H. Li, T. Zhai, Adv. Mater. 29 (2017) 1-25.
- [19] X. Fu, F. Dunne, M. Chen, W.H. Zhong, Nanoscale 12 (2020) 5483-5493.
- [20] M. Zhu, J. Wu, B. Liu, W.H. Zhong, J. Lan, X. Yang, G. Sui, J. Memb. Sci. 588 (2019) 117194.
- [21] R. Xu, X.B. Cheng, C. Yan, X.Q. Zhang, Y. Xiao, C.Z. Zhao, J.Q. Huang, Q. Zhang, Matter 1 (2019) 317–344.
- [22] C. Brissot, M. Rosso, J.N. Chazalviel, S. Lascaud, J. Power Sources 81 (1999) 925–929.
- [23] R. Xu, Y. Xiao, R. Zhang, X.B. Cheng, C.Z. Zhao, X.Q. Zhang, C. Yan, Q. Zhang, J.Q. Huang, Adv. Mater. 31 (2019) 1–8.
- [24] M. Chen, X. Fu, Z. Chen, J. Liu, W.H. Zhong, Adv. Funct. Mater. 31 (2020) 2006744.
- [25] J. Liu, F.O. Dunne, X. Fan, X. Fu, W.H. Zhong, Sep. Purif. Technol. 229 (2019) 115837.
- [26] G.H. An, H. Kim, H.J. Ahn, Appl. Surf. Sci. 463 (2019) 18-26.
- [27] J. Zhang, Y. Cai, Q. Zhong, D. Lai, J. Yao, Nanoscale 7 (2015) 17791-17797.
- [28] P. Song, X. Shen, W. He, L. Kong, X. He, Z. Ji, A. Yuan, G. Zhu, N. Li, J. Mater. Sci. Mater. Electron. 29 (2018) 12206–12215.
- [29] H. Wang, Y. Wang, P. Zheng, Y. Yang, Y. Chen, Y. Cao, Y. Deng, C. Wang, ACS Sustain. Chem. Eng. 8 (2020) 12799–12808.
- [30] D.W. Choi, K.L. Choy, Mater. Des. 191 (2020) 108669.
- [31] S. Kim, Y.K. Jeong, Y. Wang, H. Lee, J.W. Choi, Adv. Mater. 30 (2018) 1-8.
- [32] X. Fu, Y. Wang, X. Fan, L. Scudiero, W.H. Zhong, Small 14 (2018) 1803564.

- [33] Y. Tang, J. Deng, W. Li, O.I. Malyi, Y. Zhang, X. Zhou, S. Pan, J. Wei, Y. Cai, Z. Chen, X. Chen, Adv. Mater. 29 (2017) 1-10.
- [34] M. Chen, Z. Chen, X. Fu, W.H. Zhong, J. Mater. Chem. A 8 (2020) 7377–7389.
- [35] Y.H. Song, K.J. Wu, T.W. Zhang, L.L. Lu, Y. Guan, F. Zhou, X.X. Wang, Y.C. Yin, Y.
- H. Tan, F. Li, T. Tian, Y. Ni, H. Bin Yao, S.H. Yu, Adv. Mater. 31 (2019) 1–7.
  [36] L. Nie, Y. Li, S. Chen, K. Li, Y. Huang, Y. Zhu, Z. Sun, J. Zhang, Y. He, M. Cui, S. Wei, F. Qiu, C. Zhong, W. Liu, ACS Appl. Mater. Interfaces 11 (2019) 32373–32380.
- [37] J. Xiao, Q. Li, Y. Bi, M. Cai, B. Dunn, T. Glossmann, J. Liu, T. Osaka, R. Sugiura, B. Wu, J. Yang, J.G. Zhang, M.S. Whittingham, Nat. Energy 5 (2020) 561–568. [38] X. Fu, W.H. Zhong, Adv. Energy Mater. 9 (2019) 1–41.
- [39] X. Fu, C. Li, Y. Wang, L.P. Kovatch, L. Scudiero, J. Liu, W. Zhong, ACS Appl. Mater. Interfaces 10 (2018) 4726-4736.
- [40] L. Fan, S. Wei, S. Li, Q. Li, Y. Lu, Adv. Energy Mater. 8 (2018) 1702657.
- [41] X. Wang, X. Fu, Y. Wang, W. Zhong, Polymer (Guildf) 106 (2016) 43-52.
- [42] A. Bachmann, D. Wildemann, F. Praetorius, G. Fischer, T. Kiefhaber, Proc. Natl. Acad. Sci. U.S.A. 108 (2011) 3952-3957.
- [43] K. Kerman, A. Luntz, V. Viswanathan, Y.-M. Chiang, Z. Chen, J. Electrochem. Soc. 164 (2017) A1731-A1744.
- [44] Y.L. Su, J. Wang, H.Z. Liu, Macromolecules 35 (2002) 6426-6431.
- [45] S. Ali, Z. Khatri, K.W. Oh, I.S. Kim, S.H. Kim, Macromol. Res. 22 (2014) 971–977.
- [46] S. Ito, M. Iwaki, S. Sugita, R. Abe-Yoshizumi, T. Iwata, K. Inoue, H. Kandori, J. Phys. Chem. B 122 (2018) 165-170.

- [47] B.W. Zewde, L. Carbone, S. Greenbaum, J. Hassoun, Solid State Ionics 317 (2018) 97-102.
- [48] R. Arnaud, D. Benrabah, J.Y. Sanchez, J. Phys. Chem. 100 (1996) 10882-10891.
- [49] M. Ravindar Reddy, A.R. Subrahmanyam, M. Maheshwar Reddy, J. Siva Kumar, V. Kamalaker, M. Jaipal Reddy, Mater. Today Proc. 3 (2016) 3713-3718.
- [50] Y. Wang, B. Li, J. Ji, A. Eyler, W.H. Zhong, Adv. Energy Mater. 3 (2013) 1557-1562.
- [51] J.W. Lawton, Am. Assoc. Cereal Chem. 69 (1992) 351-355.
- [52] W. Li, Y. Pang, J. Liu, G. Liu, Y. Wang, Y. Xia, RSC Adv. 7 (2017) 23494–23501.
- [53] Y. Zhou, X. Zhang, Y. Ding, J. Bae, X. Guo, Y. Zhao, G. Yu, Adv. Mater. 32 (2020) 1\_8
- [54] P. Argos, K. Pedersen, M.D. Marks, B.A. Larkins, J. Biol. Chem. 257 (1982) 9984-9990
- [55] D. Xu, Z.L. Wang, L.L. Zhang, X.B. Zhang, Chem. Commun. 48 (2012) 6948-6950.
- [56] X. Chen, M. Vörös, J.C. Garcia, T.T. Fister, D.B. Buchholz, J. Franklin, Y. Du, T.C. Droubay, Z. Feng, H. Iddir, L.A. Curtiss, M.J. Bedzyk, P. Fenter, ACS Appl. Energy Mater 1 (2018) 2526-2535.
- [57] J. Jang, I. Kang, J. Choi, H. Jeong, K.W. Yi, J. Hong, M. Lee, Angew. Chemie Int. Ed. 59 (2020) 14473-14480.